Meridional circulation across the Antarctic Circumpolar Current serves as a double ^{231}Pa and ^{230}Th trap

Michiel Rutgers van der Loeff[a*], Celia Venchiarutti[a,b], Ingrid Stimac[a],

Jan van Ooijen[c], Oliver Huhn[d], Gerd Rohardt[a], Volker Strass[a]

a Alfred Wegener Institut, Helmholz Center for Polar and Marine Research, PO Box 120161, D 27515 Bremerhaven, Germany.

b now at European Commission-Joint Research Centre- Institute for Reference Materials and Measurements (IRMM), Retieseweg 111, 2440 Geel, Belgium

c Royal Netherlands Institute for Sea Research, PO Box 59, NL 1790 AB Den Burg, Texel, Netherlands

d Institute for Environmental Physics, Universität Bremen, Postfach 33 04 40, D-28334 Bremen, Germany

* Corresponding author, email mloeff@awi.de

paper accepted for Earth and Planetary Science Letters, doi: 10.1016/j.epsl.2016.07.027

Abstract

Upwelling of Circumpolar Deep Water in the Weddell Gyre and low scavenging rates south of the Antarctic Circumpolar Current (ACC) cause an accumulation of particle reactive nuclides in the Weddell Gyre. A ventilation/reversible scavenging model that successfully described the accumulation of ^{230}Th in this area was tested with other particle reactive nuclides and failed to adequately describe the depth-distributions of ^{231}Pa and ^{210}Pb. We present here a modified model that includes a nutrient-like accumulation south of the Antarctic Polar Front in an upper meridional circulation cell, as well as transport to a deep circulation cell in the Weddell Gyre by scavenging and subsequent release at depth.

The model also explains depletion of ^{231}Pa and ^{230}Th in Weddell Sea Bottom Water (WSBW) by ventilation of newly formed deep water on a timescale of 10 years, but this water mass is too dense to leave the Weddell Gyre.

In order to quantify the processes responsible for the ^{231}Pa- and ^{230}Th- composition of newly formed Antarctic Bottom Water (AABW) we present a mass balance of ^{231}Pa and ^{230}Th in the Atlantic sector of the Southern Ocean based on new data from the GEOTRACES program. The ACC receives 6.0±1.5 x 10^6 dpm s^{-1} of ^{230}Th from the Weddell Sea, similar in magnitude to the net input of 4.2±3.0 x 10^6 dpm s^{-1} from the north. For ^{231}Pa, the relative contribution from the Weddell Sea is much smaller, only 0.3±0.1 x 10^6, compared to 2.7±1.4 x 10^6 dpm s^{-1} from the north. Weddell Sea Deep Water (WSDW) leaving the Weddell Gyre northward to form AABW is exposed in the ACC to resuspended opal-rich sediments that act as efficient scavengers with a Th/Pa fractionation factor F ≤ 1. Hydrothermal inputs may provide additional removal with low F. Scavenging in the full meridional circulation across the opal-rich ACC thus acts as a double ^{231}Pa and ^{230}Th trap that preconditions newly formed AABW.

Keywords

^{231}Pa

^{230}Th

Weddell Sea

Antarctic Bottom Water

GEOTRACES

scavenging

51

Introduction

The pair of long-lived radionuclides ^{231}Pa and ^{230}Th is well suited for paleoceanographic interpretations. These nuclides are produced at a constant rate in the water from their respective U parents, ^{235}U and ^{234}U. Both are rapidly removed from the water column by scavenging but differences in their reactivities cause the two to be fractionated by particle flux, particle composition, and ocean circulation with the result that their activity ratio in surface sediments deviates from the production ratio of 0.093 (Anderson et al., 1983). The original interpretation of ^{231}Pa and ^{230}Th accumulation in sediments of the Southern Ocean was based on boundary scavenging. DeMaster (1981) interpreted high ^{231}Pa and ^{230}Th accumulation rates in the opal belt of the South Atlantic as indicative of high productivity, and the ^{231}Pa/^{230}Th ratio in Holocene and LGM sediments was used by Kumar et al. (1995) as indication for glacial-interglacial changes in the zones of high productivity. Yu et al. (1996) demonstrated that ^{231}Pa produced in the Atlantic Ocean was deposited in the opaline sediments of the ACC, paving the way to use the isotope ratio as a proxy for meridional overturning circulation (MOC).

This proxy builds on the idea that the ^{231}Pa/^{230}Th ratio in deep waters increases with water mass age and that it is reflected in the ^{231}Pa/^{230}Th ratio in deposited sediments. Glacial-Interglacial changes in ^{231}Pa/^{230}Th ratios in North Atlantic sediments have been interpreted to show changes in North Atlantic Deep Water (NADW) flow (McManus et al., 2004). Cores recovered from the South Atlantic at 2440 and 3213m, now bathed in NADW, were covered by Southern Component Water (SCW) during the Last Glacial Period (LGP) and their LGP ^{231}Pa/^{230}Th ratios have been interpreted in terms of northward flow (Jonkers et al., 2015; Negre et al., 2010). Similarly, south Atlantic cores from greater depth are expected to record the history of AABW flow (Lippold et al., 2016). Interpretations in terms of northward flow of SCW or AABW depend on assumptions on the scavenging history and resulting preformed ^{231}Pa/^{230}Th

ratio in these southern source waters (Jonkers et al., 2015; Lippold et al., 2016; Negre et al., 2010). Considering that the $^{231}Pa/^{230}Th$ ratio in newly deposited particles is largely determined by the lower 1000m of the water column (Thomas et al., 2006) and that wide areas of the abyssal sediments are bathed in AABW, it is important to know what controls the ^{231}Pa and ^{230}Th activities in freshly produced AABW. A large part of AABW enters the ACC from the Weddell Gyre as Weddell Sea Deep Water (WSDW), whether it is produced in the Gyre (according to a traditional estimate 60-70% of AABW, Orsi et al., 1999; Orsi et al., 2002) or advected in the coastal current from the Indian Ocean (Hoppema et al., 2001; Jullion et al., 2014; Meredith et al., 2000). The processes controlling the $^{231}Pa/^{230}Th$ ratio in the WSDW are therefore important for the interpretation of the ratio in deep water sediments at lower latitudes as proxy for MOC (Anderson et al., submitted in parallel).

According to the classical reversible scavenging model, the activities of dissolved and particulate $^{230}Th_{xs}$ and $^{231}Pa_{xs}$ increase linearly with depth (Bacon and Anderson, 1982; Nozaki et al., 1981) , where the subscript xs means excess activities, i.e. the activities of nuclides produced by U decay in seawater. Although all activities presented here are excess activities, we will, following Deng et al. (2014), leave out the subscript in this paper. Rutgers van der Loeff and Berger (1993) reported ^{230}Th and ^{231}Pa profiles from the Weddell Gyre that reached maximum concentrations at mid-depth, and showed how the distribution of these isotopes was controlled by upwelling of CDW and low scavenging rates in these waters south of the ACC characterized by low particle flux (Fischer et al., 1988).

The scavenging of Pa depends strongly on the opal flux. The F ratio (scavenging preference of Th over Pa) changes dramatically through the ACC. North of the ACC the F ratio is 10 or higher, whereas in the opal belt and south of it Pa is much more strongly scavenged than further north, giving an F ratio <1 (Chase et al., 2002; Walter et al., 1997). The change in F ratio across the ACC is a circumpolar phenomenon. Chase et al. (2003) gave a detailed description of the change in the south Pacific based on

98 water, surface sediment and sediment trap data. They showed that, in this area of the Pacific with little
99 deep water formation, the activities of ^{230}Th and ^{231}Pa show no significant gradients on isopycnal
100 surfaces implying that the upwelling and isopycnal ventilation are too rapid to allow changes in nuclide
101 activities in the upwelled water masses. In the Atlantic sector, upwelled deep waters have a long
102 residence time in the Weddell Gyre under a low-scavenging regime, and although we know that ^{230}Th
103 accumulates under these circumstances (Rutgers van der Loeff and Berger, 1993), it has not yet been
104 clearly shown whether the low scavenging regime with a low F ratio also allows ^{231}Pa to accumulate.

105 Recently, new data on the distribution of ^{230}Th, ^{231}Pa and ^{232}Th have become available in the GEOTRACES
106 program. Venchiarutti et al. (2011a) described the distribution of these nuclides in Drake Passage and so
107 constrained the composition of Pacific waters transported in the ACC. Deng et al. (2014) quantified the
108 transport of ^{231}Pa and ^{230}Th with NADW into the Southern Ocean. Venchiarutti et al. (2011b) gave new
109 data from Weddell Gyre and Zero Meridian. With this widely improved dataset we now have a firm basis
110 to address the following questions:

111 - What controls the accumulation of ^{230}Th and ^{231}Pa in the Weddell Gyre and especially in WSDW?
112 - What controls the composition of ^{230}Th and ^{231}Pa in AABW exported from the Weddell Gyre and
113 across the ACC to the abyssal ocean?
114 - What is the fate of the ^{230}Th and ^{231}Pa imported in the SO with NADW (Deng et al., 2014) and
115 what is the mass balance of ^{230}Th and ^{231}Pa in the Atlantic sector of the Southern Ocean?

116 In this paper, we present a model to explain the observed distributions of ^{230}Th and ^{231}Pa in the Weddell
117 Gyre, check the model by applying it to another particle reactive nuclide (^{210}Pb) and give a mass balance
118 of ^{230}Th and ^{231}Pa in the Atlantic sector of the Southern Ocean. We argue that the ACC functions as a
119 double trap for ^{230}Th and ^{231}Pa, once in the surface water and once again in the outflowing deep water.

120

Hydrography of the Weddell Gyre and adjacent ACC:

In the Southern Ocean, shoaling Circumpolar Deep Water (CDW) feeds into a shallow meridional overturning cell, upwelling into surface waters and leading to the formation of intermediate waters, and into a deep cell transforming CDW and forming Antarctic Bottom Water (Chase et al., 2003; Fahrbach et al., 2011, Fig. 2). The transport is overwhelmed by the zonal transport in the ACC.

In the Weddell Gyre, CDW enters from the east and circulates as what is locally known as Warm Deep Water (WDW) at depths of 200-1500m. WDW with at its core a neutral density anomaly of 27.88 kg m^{-3} is primarily of Lower Circumpolar Deep Water (LCDW) density. Dense waters are produced by ice formation on the continental shelf (high salinity shelf water, HSSW) and under the ice shelf (Ice Shelf Water, ISW). WDW mixes with these salinified and cooled shelf waters to form Weddell Sea Bottom Water (WSBW) and the somewhat less dense WSDW. When these newly formed deep waters leave the Weddell Gyre they are the source of the circumpolar AABW that fills the abyssal ocean.

The Weddell-Enderby basin has a cyclonic circulation with a strong recirculation in the western part (Fahrbach et al., 2011). The basin is confined by a ridge system in the north, and deep and bottom waters can only leave the basin through gaps in these ridges. Outflows of WSDW to the ACC and beneath the ACC to the Argentine Basin are observed over the south Scotia Sea and Georgia Basin, and over the Enderby Basin toward the Crozet-Kerguelen Gap (Haine et al., 1998; Orsi et al., 1999; Orsi et al., 1993) (Fig. 1). About half of the export of WSDW occurs through the gaps in the Scotia Ridge (Jullion et al., 2014; Naveira Garabato et al., 2002). This deep water, that exits through the Georgia Passage and Georgia Basin into the Argentine Basin, is more ventilated, cooler and fresher, with origins rather on the slope of the Antarctic Peninsula, whereas the WSDW leaving further east is derived from the Filchner-Ronne Ice Shelf (Gordon et al., 2001; Naveira Garabato et al., 2002).

Upwelling, circulation and scavenging: the behavior of particle-reactive nuclides in the Weddell Gyre

The distribution of ^{230}Th in the Weddell Gyre has been measured during Polarstern expedition ANT-VIII/3 in 1991 by Rutgers van der Loeff and Berger (1993) and more recently during Polarstern expedition ANT-XXIV/3 (PS71) in 2008 by (Venchiarutti et al., 2011a; Venchiarutti et al., 2011b) (Fig 1). Positions and references for all stations discussed in this paper are given in Table S1. The ^{230}Th distribution in the Weddell Gyre was explained by Rutgers van der Loeff and Berger (1993) using a model that combined a simple representation of southward upwelling of ^{230}Th-rich LCDW across the ACC in the Antarctic divergence with reduced scavenging in relation to the very low particle fluxes in the Weddell Gyre. Further evidence for this reduced scavenging rate was provided by sediment trap data (Fischer et al., 1988) and sediment trap and - core analyses by Walter et al. (2000).

In addition, it was shown that in the deepest water layer where potential temperature θ <-0.7°C and the water mass is characterized by Weddell Sea Bottom Water, ^{230}Th activities are lower than at mid-depth (observed both in the 1991 and the 2008 dataset), a feature not represented in the model of Rutgers van der Loeff and Berger (1993). In principle, this decline can be caused by two mechanisms: either by seafloor scavenging, as has been proposed in several other deep-sea environments (Deng et al., 2014; Hayes et al., 2015a; Jeandel et al., 2015), or by ventilation with new bottom water formation as already suggested by Rutgers van der Loeff and Berger (1993). Fig. 3 shows the effect of ventilation by bottom water formation on the distribution of ^{230}Th compared with ^{230}Th data of station 193 of Polarstern expedition ANTXXIV-3 in 2008 (Venchiarutti et al., 2011b) (Fig.1, Table S1). The composition of the bottom water was derived from an Optimum Multiparameter Analysis (OMP) based on potential temperature, salinity, helium isotope, neon data collected during ANTXXIV-3 (applying the same approach and parameter setting to the 2008 data as described in Huhn et al., 2008). This analysis showed that in the vicinity of station 193, at station 196 (datapoint with available He isotope and Ne

data closest to station 193, Fig. 1, Table S1) the bottom water consisted of 46±5% Warm Deep Water (WDW), 38±13% High Salinity Shelf Water (HSSW), 8±7% Ice Shelf Water (ISW) and 8±3% surface water. For WDW with potential temperature of 0.44°C, we interpolate from the experimental profile a dissolved ^{230}Th concentration of 1.14 dpm m^{-3}. For all surface water components, including ISW and HSSW, we use the ^{230}Th activity that we found at 50m depth on Sta 193 (0.18 dpm m^{-3}), which compares well with the activities found by Fleisher and Anderson (2003) at the end of summer in the Ross Sea. For recently ventilated WSBW, we find a dissolved ^{230}Th activity of 0.65 dpm m^{-3}. In Fig.3, we show that it takes about 10 years before ingrowth and reversible exchange with settling particles cause this activity to increase to the measured value of 1.2 dpm m^{-3}. This result is in reasonable agreement with the transient tracer (chlorofluorocarbons, CFC) based Transit Time Distribution as calculated by Huhn et al. (2013), which gives the most likely age of 20±5 years of the bottom water at station 193.

Now that the ^{230}Th data can be reasonably well explained in this way (Fig.3), we check whether the model also adequately describes the distributions of other particle-reactive nuclides. We therefore apply the model to ^{231}Pa and ^{210}Pb, using upwelling of deep waters north of the Antarctic Polar Front (APF) with the composition as given by Venchiarutti et al. (2011b) for ^{231}Pa and by Somayajulu and Craig (1976) for ^{226}Ra and ^{210}Pb. We use a vertical mixing rate of 5 x 10^3 m^2 y^{-1} and for ^{210}Pb an atmospheric input of 3 dpm cm^{-2} y^{-1} (Rutgers van der Loeff and Berger, 1991), but for simplicity, the input of WSBW is not included in these model runs shown in Fig. 4 (black lines). The scavenging rates of Pa and Pb are based on that of Th using for Pa a fractionation factor of F(Th/Pa)=1 (Walter et al., 1997) and for Pb in the test run F(Th/Pb) =1.

As shown from the model runs in Fig.4 (black lines), the fits for ^{231}Pa and ^{210}Pb to the experimental values found in the Weddell Sea for ^{231}Pa (Venchiarutti et al., 2011b, Sta 193) and for ^{210}Pb (Somayajulu and Craig , 1976, GEOSECS Station 89) are very poor. Indeed, the model developed for ^{230}Th fails here to

reproduce the very shallow maximum in dissolved ^{210}Pb and produces far too low activities of ^{231}Pa. In order to improve the model and especially to better represent the much shallower accumulation of ^{231}Pa and ^{210}Pb compared to ^{230}Th we must investigate in more detail what controls the scavenging process in the Weddell Gyre.

A closer look at particle rain and mineralization in the Weddell Gyre:

shallow mineralization

The sedimentary record shows high recent opal sedimentation rates just south of the Southern Polar Front (Geibert et al., 2005) and it has generally been assumed that productivity and export fluxes are higher in this area than further south in the Weddell Sea (Fischer et al., 1988; Walter et al., 2000). Several studies using ^{234}Th in the ACC confirm the high export around the Polar Front of the southern Atlantic (Planchon et al., 2012; Rutgers van der Loeff et al., 2002; Usbeck et al., 2002), a situation also observed in the South Pacific (Buesseler et al., 2001; Buesseler et al., 2003). Further south, in the Weddell Gyre, production is thought to be limited by iron supply (Smetacek et al., 1997) and sediment accumulation rates are very low. Nevertheless, Leynaert et al. (1993) observed in the Weddell Sea biogenic silica production rates exceeding average rates in the ACC and Hoppema et al. (1999) showed from a surface layer balance that export production in the central Weddell Gyre is larger than the average for the Southern Ocean. Other studies point at blooms with high chlorophyll concentrations and high export rates at these higher latitudes (Geibert et al., 2010). This discrepancy is explained by the unusually shallow mineralization in the Gyre, as shown by ^{234}Th studies of Planchon et al. (2012) and Usbeck et al. (2002). The first authors were able to quantify ^{234}Th excess and to relate it to mineralization rates estimated from the distribution of particulate barite. They observed that the depth range for mineralization was deeper in the region bounded by the Subantarctic Front and the APF (100-600m) than in the (northern) Weddell Gyre (upper 400m). Usbeck et al. (2002) observed a ^{234}Th excess

in the depth range of just 100-200m in the Weddell Gyre, supporting the concept of an unusually shallow depth of mineralization in this basin (Leynaert et al., 1993; Whitworth and Nowlin, 1987).

Central Intermediate Water

In the central Weddell Sea, the shallow mineralization gives rise to a water layer within the Warm Deep Water characterized by low oxygen, high nitrate and total carbonate (TCO_2) (Hoppema et al., 2002; Whitworth and Nowlin, 1987), coined Central Intermediate Water (CIW) by Whitworth and Nowlin (1987). This water mass with at its core a neutral density around 27.88 $kg.m^{-3}$ is derived from LCDW with very low CFC content (Huhn et al., 2013), and is exposed to upwelling (Hoppema et al., 2002; Jullion et al., 2014) and erosion from above by entrainment into surface waters. It exchanges isopycnally with UCDW/LCDW in the north on a timescale of 3 years (Hoppema et al., 2002).

The shallow maximum in ^{210}Pb observed at GEOSECS station 89 (Somayajulu and Craig, 1976) (Fig. 4), in the core of is now called CIW, was interpreted by Farley and Turekian (1990) to be produced locally, i.e. by shallow mineralization and not by advection. Recently, Hoppema et al. (2015) confirmed that the characteristics of the CIW described by Whitworth and Nowlin (1987) with its shallow nitrate maximum indicating a maximum in remineralization rate at 200-500m depth are found consistently over many years. They also found a corresponding maximum of silicate at much larger depth: 1000-2000m, indicating that the opal skeletons dissolve at much greater depth than the organic matter. While this is a usual phenomenon in many ocean areas it is somewhat surprising to find this deep opal dissolution in the Weddell Gyre because Leynaert et al. (1993) had argued based on sediment trap data of Fischer et al. (1988) that less than 1% of biogenic silica produced in the surface water of the northern Weddell Sea reaches a depth of 800m.

In Fig. 2 we have extended the schematic meridional circulation model described by Chase et al. (2003) to include the special situation in the Weddell Gyre with its upwelling, deep water formation, and

shallow mineralization in the Central Intermediate Water. In an upper meridional circulation cell, nutrient-rich UCDW feeds the surface water and is then, on its way back north, depleted in silicate by strong diatom production and correspondingly high opal flux just south of the APF. This flux also carries ^{231}Pa to intermediate depth, preventing the ^{231}Pa to be carried north in surface waters. Instead, the cell functions as a trap for ^{231}Pa, which settles out and accumulates at intermediate depth until it is exported as WSDW and AABW. There are two reasons why this upper circulation cell is more effective in accumulating ^{231}Pa than ^{230}Th: firstly, the strong affinity of Pa to opal, and secondly, the nonlinear depth distribution of ^{231}Pa (and ^{210}Pb) north of the Polar Front. In those lower latitudes, ^{231}Pa and ^{210}Pb are relatively constant from 1500m downwards, whereas ^{230}Th continues to increase linearly with depth. The UCDW that upwells from mid-depth has approximately the same ^{231}Pa and ^{210}Pb activities but only half the ^{230}Th activities if compared to water from full depth. In Fig.5, we have modified the model of Rutgers van der Loeff and Berger (1993) of the nuclide activity profile in the Weddell Sea to take into account the processes shown in Fig.2 that are essential aspects in the scavenging of ^{231}Pa and ^{210}Pb. The modified model still includes a renewal of WSDW by LCDW on a time scale of 35 years, but is now extended with the rapid exchange of WDW/CIW (100-500m) with UCDW/LCDW from N of Polar Front and with the input of WSBW as described above (Fig. 3). The composition of recently produced WSBW is derived in analogy to the procedure followed for ^{230}Th. For WDW we find ^{231}Pa and ^{210}Pb concentrations of 0.35 and 140 dpm m^{-3}, and for recently formed WSBW concentrations of 0.23 and 89 dpm m^{-3}, respectively. Upwelling is set at 33m yr^{-1} (Hoppema et al., 1999), an upwelling rate that, within the large errors in the budget for surface water layer, is supported by the analysis of Jullion et al. (2014). The composition in the northern box is assumed to be set by the circumpolar current and is not changed in the model.

The Th data are well represented if the scavenging process is described by a constant particle flux and reversible scavenging (as in Rutgers van der Loeff and Berger, 1993) (Fig. 4). The modified model gives a

better representation of the ^{231}Pa and ^{210}Pb profiles than the original model, provided we allow the fractionation factor to change with depth. The fractionation factors in deep waters are constrained by the nuclide ratios observed in surface sediments (Table S2). We find the best fit with observations for an 8 times higher scavenging rate in surface waters for both Pa and Pb, decreasing with depth with a relaxation depth of 2000m and 250m, respectively (Fig. 4). All model parameter values are listed in Table S2. These three different scavenging depth regimes seem to be related to a combination of different particle fluxes: a component with shallow mineralization that releases ^{210}Pb at shallow depth, an opal flux that carries ^{231}Pa to depth where it is released upon opal dissolution (Hoppema et al., 2015), and a third component that is not mineralized and sinks to the seafloor. The shallow release of ^{210}Pb points at a relationship with the mineralization of organic matter. The strong increase in the Th/Pa fractionation factor with depth (here from 0.36 to 2.9) has also been applied in 2D-scavenging models of the Atlantic MOC (Lippold et al., 2012; Luo et al., 2010) and is in agreement with other data from the Southern Ocean. Venchiarutti et al. (2011a) reported reduced F ratios in the surface 500m in the Drake Passage, and from sediment trap results Chase et al. (2003) found a higher F ratio at depth than in surface waters. F ratios calculated using ^{231}Pa/^{230}Th ratios in surface sediments increase with depth off Southwest Africa (Scholten et al., 2008). However, using suspended particles, these latter authors found a broad maximum in fractionation factor for the water column between ~1000m and 4400m off Southwest Africa, which fits with the observations of Moran et al. (2002) in the Argentine Basin. Conversely, Hayes et al. (2015b) observed an opposite depth dependence in the North Atlantic Ocean, a difference that is probably due to the minor role played by opal in their study.

A mass balance of ^{230}Th and ^{231}Pa in the Atlantic sector of the Southern Ocean

Further constraints on the ^{231}Pa and ^{230}Th activities in deep water leaving the Weddell Gyre as WSDW/AABW can be based on mass balance considerations. A mass balance for ^{230}Th and ^{231}Pa for the

Southern Ocean presented by Chase et al. (2003) describes the fluxes of these nuclides across the APF for all three ocean basins. In the Atlantic sector of the Southern Ocean, the region south of the APF consists of two widely different zones: the northern part, between the APF and the Southern Boundary, is part of the ACC with large export production, high diatom production and opal sedimentation (the opal belt). South of the Southern Boundary we find the Weddell Gyre with low flux and low burial. In order to make a mass balance of the Atlantic sector we refine the mass balance presented by Chase et al. (2003) by separating the ACC from the Weddell Gyre.

Our analysis is based on the circulation of the Atlantic Sector of the Southern Ocean as given by Sloyan and Rintoul (2001). From their analysis of hydrographic data (cruise tracks shown in Fig. 1) we use the meridional fluxes across the SAVE 4 and Wedsea transects, the net zonal fluxes to the Indian (across AJAX transect) and Pacific (across Drake Passage) Oceans, and the diapycnal fluxes across the neutral density surfaces 27.4, 28.0 and 28.2 $kg.m^{-3}$ (Sloyan and Rintoul, 2001, their Fig. 13, Table 1). The Wedsea transect of the AJAX expedition separates the ACC from the Weddell Sea. Total volumes defined by the sections were calculated with a matlab program using the published coordinates of the sections (Ajax, DrakeP and SAVE4) for the area and the ETOPO05 database (NOAA, 1988) for the depth. Nuclide fluxes for each water mass are calculated as the product of the mass flux and the literature value of their nuclide activities (Table 2).

Mass balance of Weddell Gyre

We start with a mass balance of the Weddell Gyre. In the density range <28.0 $kg.m^{-3}$ (Table 1) a southward transport of about 1 Sverdrup (10^6 m^3 s^{-1}, Sv) of upwelling NADW is balanced by a northward transport of surface water (AASW). Due to the difference in activity of the nuclides this implies a net southward transport of 0.2±0.2 x 10^6 dpm s^{-1} of both ^{230}Th and ^{231}Pa. As a result of the strong accumulation of ^{230}Th and ^{231}Pa in deep waters in the Weddell Gyre (γ^n >28.0 $kg.m^{-3}$) the outflowing

deep waters have higher concentrations of ^{230}Th and ^{231}Pa than the inflowing waters. Simple mass balance requires that the cumulative nuclide flux in inflowing waters with concentration A_{in} plus in situ production P is balanced by outflowing waters with concentration A_{out} plus burial B.

$$\Sigma F(A_{in}-A_{out}) + P = B$$

The production of ^{230}Th in the Weddell Gyre is given by

$$P_{230} = \lambda_{230} V_{Weddell}$$

and similarly for ^{231}Pa

$$P_{231} = \lambda_{231} V_{Weddell}$$

Where λ_{230} and λ_{231} are the decay constants of ^{230}Th and ^{231}Pa. With a water volume $V_{Weddell}$ in the Weddell Gyre south of the Wedsea transect (Fig. 1) of 1.22 x 10^{16} m^3, we thus have a direct relationship between burial/production (B/P) ratio, the water flow F and the increase in concentration A.

Sloyan and Rintoul (2001) described the exchange through the Wedsea transect as a southward transport of 11 Sv of deep waters consisting of 4 Sv in the density range LCDW (28.0-28.2 kg.m^{-3}) and 7 Sv with density >28.2 kg m^{-3} balanced by a northward transport of 11 Sv of WSDW/AABW (γ^n >28.2 kg m^{-3}). The estimates of the net production rate of WSDW/AABW in the Weddell Gyre vary widely. More recently, Jullion et al. (2014) mentioned an export of AABW to the north of 8±2 Sv of which 6±2 Sv is produced in the Weddell Gyre, the remainder being imported from the east. In a first analysis we disregard this input from the Indian Ocean (see arguments below) and describe the deep water circulation of the Weddell Gyre as an input of 8 Sv in the LCDW density range and an export of 8 Sv as WSDW.

Following the analysis of Chase et al. (2003), we define characteristic concentrations for the water masses (Table 2). LCDW flowing south has ^{230}Th and ^{231}Pa activities of 1.0 dpm m^{-3} and 0.35 dpm m^{-3} (Rutgers van der Loeff and Berger, 1993). For the WSDW/AABW density range (γ^n >28.2 kg m^{-3}) we distinguish three water types: the waters found in the western (WSDWW) and central/eastern (WSDWE) Weddell Gyre and the AABW observed by Deng et al. (2014) in the Argentine Basin (AABWA), taken to be representative for the AABW transport across SAVE4(Table 2).

For the AABW/WSDW transport across the Wedsea transect, we consider two extreme options. Firstly, in the perimeter and in the western part of the Weddell Gyre (WSDWW: Venchiarutti et al., 2011a, Sta 236) ^{230}Th and ^{231}Pa activities are 1.5 and 0.4 dpm m^{-3}, respectively, resulting in a net northward (export) flux of 3.8±4.0 and 0.2±1.1 x 10^6 dpm.s^{-1} for ^{230}Th and ^{231}Pa respectively, and respective B/P ratio in the Weddell Gyre of 0.62 and 0.78). However, if we take the high activities measured in the central Gyre (WSDWE: 1.9 and 0.6 dpm m^{-3} for ^{230}Th and ^{231}Pa, respectively) to be representative for the 8 Sv of WSDW flowing north, we find an export of 7.0 and 1.8 x 10^6 dpm s^{-1} with a B/P ratio in the Gyre of 0.3 and -0.9, respectively. In the latter case, the export of ^{231}Pa exceeds the combined import and in situ production, which in steady state is not possible. In other words, the northward outflowing WSDW/AABW must have a lower ^{231}Pa concentration.

Inverting the argument, we can start with the observation of Walter et al. (2000) who found a B/P ratio in the central Gyre of 0.4 for ^{230}Th. The ^{231}Pa/^{230}Th ratio on suspended particles and in surface sediments far south of the APF is constant at 0.15±0.03 (Walter et al., 1997)(Latitude > 55°S, depth>1000m, http://doi.pangaea.de/10.1594/PANGAEA.54596) and the ^{231}Pa/^{230}Th production ratio is 0.093, implying that for ^{231}Pa the present B/P ratio is 0.65. Using for ^{230}Th a B/P ratio of 0.4±0.15 and for ^{231}Pa a B/P ratio of 0.65±0.15, we find that a deep water flow of 8 Sv is enriched by 0.75±0.27 dpm m^{-3} in ^{230}Th, a value in agreement with the analysis of Rutgers van der Loeff and Berger (1993) (Sta 227) and within the range

of observations of Venchiarutti et al. (2011b)(Stations 131, 193). An analogous argument for ^{231}Pa shows that the outflowing deep water is enriched by only 0.04±0.02 dpm m^{-3}. This increase is small compared to the range of activities observed in deep waters. The available data of the Weddell Gyre do not allow to define the concentration in the outflow with sufficient accuracy to use them to calculate the net outflow of ^{231}Pa to the north. The mass balance of the Weddell Gyre is a more appropriate way to define the net northward loss of ^{231}Pa. Based on this mass balance consideration, we find that the export of ^{230}Th and ^{231}Pa from the Weddell Gyre to the north is 6.0±1.5 and 0.32±0.14 x 10^6 dpm s^{-1}, respectively (Fig. 6).

The above calculation showed that the high activity of ^{231}Pa observed in the central Weddell Sea (>0.6 dpm m^{-3}, Sta 131, 193) cannot be representative for the water masses leaving the Weddell Gyre as WSDW/AABW. Indeed there are large horizontal gradients in the Weddell Gyre with higher CFC (Huhn et al., 2013) and lower concentrations of Ba (Hoppema et al., 2010), ^{231}Pa (Venchiarutti et al., 2011b), TCO_2 (Hoppema et al., 2002) in the perimeter of the Gyre, and lower CFC and higher accumulation in the center of the Gyre. We conclude that the exported water masses are derived from the outer reaches of the gyre characterized by lower concentrations, whereas the central water masses have a longer residence time allowing further accumulation of mineralization products (Ba, TCO_2) and isotopes produced by in situ production (^{230}Th, ^{231}Pa).

This contrast is enhanced by the import from the Indian. The large input associated with the Antarctic Slope Front (ASF), 14 Sv of CDW and 9 Sv of WSDW (Jullion et al., 2014) with relatively low ^{231}Pa concentrations (Venchiarutti et al., 2011b, Sta 178) can only have very limited exchange with the high-^{231}Pa waters in the central Weddell Sea. If an appreciable part of this input from the East mixed into the central waters of the gyre, the high ^{231}Pa observed there would imply an export far in excess of the production rate. The Indian input must consequently largely be a through-flow, modified by its

interaction with Weddell Sea water masses, and exiting towards the ACC in the north (Jullion et al., 2014).

Mass balance of Atlantic sector of the ACC including the opal belt

The mass balance of nuclides in the Atlantic sector of the ACC is calculated from the water transports and nuclide concentrations in Tables 1 and 2, respectively. Our estimates of nuclide fluxes across SAVE 4 (Fig. 6) are somewhat lower than the estimates made by Deng et al. (2014) who gave a southward flux of 6.35 x 10^6 dpm s^{-1} for ^{230}Th and 3.57 x 10^6 dpm s^{-1} for ^{231}Pa. Deng et al. (2014) based their estimate on the hydrographical analysis of Vanicek and Siedler (2002) who use slightly different density limits of the water masses and give different fluxes compared to Sloyan and Rintoul (2001). For the estimation of the nuclide transport across the Wedsea transect, we use the mass balance considerations for the Weddell Gyre south of the Wedsea transect as presented above.

The resulting activity balance for the entire water column (Fig. 6) shows that a net amount of 11.2 x 10^6 dpm s^{-1} of ^{230}Th and 1.8 x 10^6 dpm s^{-1} of ^{231}Pa is imported into the region between the hydrographic sections SAVE 4, Wedsea, DrakeP and AJAX. This activity accumulates in the sediment together with the activity produced within the area (3.1 x 10^7 and 2.9 x 10^6 dpm s^{-1} for ^{230}Th and ^{231}Pa, respectively, assuming a volume of 3.81 x 10^{16} m^3). This results in a B/P ratio of 1.36 and 1.65 for ^{230}Th and ^{231}Pa, respectively (Fig. 6), which is in good agreement with an earlier estimate of the B/P ratio for ^{230}Th in the Atlantic sector of the ACC in the range 1.12-1.42 (Walter et al., 2000). The calculated burial ^{231}Pa/^{230}Th activity ratio is 0.11 (Fig.6), well in excess of the production ratio of 0.093. In this area a strong latitudinal gradient exists in ^{231}Pa/^{230}Th activity ratios in suspended particles and in surface sediments from <0.093 north of the APF to >0.093 south of it (Walter et al., 1997). The much higher sediment rain rates south of the APF (Geibert et al., 2005) explain why the average burial ^{231}Pa/^{230}Th activity ratio exceeds the production ratio.

The net nuclide transport to the Indian and Pacific oceans has a large error because small concentration changes in the ACC (130 Sv) between the Drake and Zero Meridian transects would cause a large source or sink in the area. As already mentioned by Walter et al. (1997) it is difficult to estimate what part of the additional nuclide sedimentation is exported to the Indian Ocean.

The budget of ^{231}Pa is strongly affected by the large southward transport of ^{231}Pa from the Argentine basin (Deng et al., 2014; Yu et al., 1996), whereas the export from the Weddell Gyre is comparatively small. The input of ^{231}Pa from the north causes a large excess sedimentation in the opal belt.

The low ^{230}Th activities found by Deng et al. (2014) in the AABW in the Argentine Basin make the temperate South Atlantic also a source of ^{230}Th for the ACC. The export from the Weddell Gyre is of the same magnitude as the supply from the north. If, as assumed in our analysis, all excess is deposited in the Atlantic sector of the ACC and not transported to the Indian Ocean, the B/P ratio is 1.36 (Fig.6), at the high end of the range for ^{230}Th sedimentation given by Henderson et al. (1999) and to be considered when using ^{230}Th for flux normalization.

This mass balance in the Atlantic Ocean sector is very different from the circumpolar average fluxes across the APF for which Chase et al. (2003) found an appreciable net southward transport of ^{231}Pa and a relatively small net northward transport of ^{230}Th.

Export of ^{231}Pa and ^{230}Th in AABW: indications of removal in bottom waters

While WSBW (θ<-0.7°C, density > 28.4 kg.m^{-3}) is locally depleted in ^{230}Th and ^{231}Pa as a result of deep water formation (Fig. 3), this water mass is too dense to leave the Weddell Gyre. Yet, WSBW is mixed vertically into WSDW and it is this overlying WSDW, strongly enriched in ^{230}Th and ^{231}Pa by accumulation in the Weddell Gyre, that is the source of AABW leaving the Weddell Gyre northward and spreading out

417 over the deep basins in the Atlantic and Indian Oceans (Fig. 1). On its way north, it loses extreme
418 characteristics and becomes less dense by mixing with overlying waters of LCDW/WDW type.

419 We take as representative for the AABW export the nuclide composition at neutral density 28.2-28.3 kg
420 m^{-3}. We have argued above that the WSDW/AABW exported from the Weddell Gyre must have ^{230}Th
421 and ^{231}Pa activities 0.75 and 0.04 dpm m^{-3} higher than in the inflowing LCDW, which results in expected
422 activities of 1.3-1.8 and 0.35-0.39 dpm m^{-3}, respectively (boxes in Fig. 8). However, we do not find these
423 high ^{230}Th and ^{231}Pa activities in AABW north of the APF (Fig. 8). In the AABW density range Deng et al.
424 (2014) found ^{230}Th and ^{231}Pa activities of 0.83 ± 0.2 and 0.28 ± 0.03 dpm m^{-3}, respectively. In the South
425 Sandwich Trench (Sta 1785) and in a 5160m deep basin east of this (Sta 1782), stations in an area of
426 outflow of AABW (Orsi et al., 1999), Rutgers van der Loeff and Berger (1993) observed dense waters
427 with in the density range 28.3< γ_n<28.4 kg.m^{-3} activities much lower than at corresponding density in the
428 Weddell Gyre (Stations 131, 193, 227), while in the AABW density range 28.2< γ_n<28.3 kg.m^{-3}) ^{230}Th and
429 ^{231}Pa activities did not exceed 1.08 and 0.35 dpm m^{-3}, respectively (Fig. 8). The densest water sampled
430 north of the APF on the Zero Meridian had a neutral density of 28.31 kg m^{-3} (in 1989) and 28.23 kg m^{-3}
431 (in 2008) (Fig. 8). Between 40-53°S, dissolved ^{230}Th activities of 0.67-1.07 and dissolved ^{231}Pa activities of
432 0.28-0.35 dpm m^{-3} were found in waters with a density exceeding 28.2 kg m^{-3} (Fig. 8). In the SW Indian
433 Ocean, Thomas et al. (2006) found 1.03 ± 0.05 (1 SE) dpm m^{-3} dissolved ^{230}Th (1.13 ± 0.06 dpm m^{-3}
434 unfiltered) at neutral density 28.22 kg.m^{-3} (at 32.6°S, WIND3) (Fig. 8). Their southernmost ^{231}Pa data
435 (unfiltered) at AABW density are from 20°S (WIND15, 4400m, γ_n = 28.26 kg m^{-3}) and were as low as 0.19
436 ± 0.01 dpm m^{-3}. The high activities found by Scholten et al. (2008) further north in the deep Cape Basin
437 appear not to be connected. They were found in water masses with neutral density <28.2 kg m^{-3} (Fig. 8)
438 and cannot be directly derived from WSDW. Deng et al. (2014) noticed that their depth profiles of ^{230}Th
439 and ^{231}Pa did not continue to increase linearly with depth until the seafloor and argued that the
440 observed near-bottom depletion reflects a removal process at or near the seafloor. A comparison with

441 the expected outflow concentrations of AABW at this density (Fig. 8) shows that an even much larger
442 nuclide removal must take place during transit of AABW from the Weddell Gyre to the latitudes N of the
443 ACC and into the Argentine Basin. This supports the observation of Thomas et al. (2006) who reported a
444 decrease of ^{231}Pa with depth below the NADW layer in the SW Indian Ocean and speculated on a
445 removal of ^{231}Pa in deep waters while they cross the opal-rich ACC.

446 The northern edge of the Weddell Gyre is characterized by mountain ranges rising to depths of approx.
447 3000m. Only a few deeper passages in the Scotia Ridge (Orkney, Bruce and Discovery Passages) and
448 further East (South Sandwich Trench) allow concentrated outflow of AABW (Fig. 1). At other longitudes,
449 there may well be north-south exchange over the mountain ranges. We know from nephelometer data
450 (Biscaye and Eittreim, 1977) that below approx. 2500m the suspended load increases with depth. The
451 strong currents associated with the ACC fronts continue to full depth and maintain a nepheloid layer
452 over the seafloor, both at abyssal depths and over the ridges.

453 A benthic nepheloid layer was observed with transmissometry at all stations when we crossed the
454 America Antarctic Ridge during the Zero and Drake expedition (Fig. S1). The transmission values in the
455 benthic nepheloid layer were lower and consequently the particle load was higher at the northern side
456 of the Ridge. In this same area a similar nepheloid layer was observed throughout during the EIFEX
457 project, carried out in 2004 (Fig. S2). The ridges are situated within the opal belt (Geibert et al., 2005)
458 which means that they are covered with opal-rich sediments. Dissolved silicate concentrations in the
459 deepest waters just over the mountains are exceptionally high (Fig. S3), which could be due to diffusion
460 from the sediments but is more likely due to opal dissolution in the suspended phase.

461 Kretschmer et al. (2011) investigated grain-size dependent adsorption of ^{231}Pa and ^{230}Th to sediments
462 from the opal belt (Shona Ridge, PS1768-8, 52.5930°S, 4.4760°E, 3299 m) and showed that the easily
463 suspended fine fraction (<20μm) and especially the diatom-rich slowly sinking coarser fraction (20-

50µm) had a high $^{231}Pa/^{230}Th$ ratio. Therefore, we conclude that the deep waters leaving the Weddell Gyre over these ridges are exposed to strong interaction with suspended opal and lose part of the ^{231}Pa and ^{230}Th that had accumulated in the Weddell Gyre. As a result of the low Pa/Th fractionation of opal, this additional bottom scavenging is relatively less effective for ^{230}Th.

An additional removal likely takes place by contact of bottom waters with hydrothermal inputs. Manganese (hydr)oxides formed around vent sites are very efficient in removing Th and Pa from the water column (Hayes et al., 2015a). We have no direct evidence for hydrothermal scavenging but many active vents have been observed along the Scotia Ridge and especially in the area of throughflow towards the Argentine basin (German et al., 2000). Venting is also apparent on the Bouvet Triple junction region near Sta 113 (Middag et al., 2011, Fig. S3) and on the Southwest Indian Ridge (Tao et al., 2012). With a Th/Pa fractionation factor of 5.5±2.8 for manganese (hydr)oxides (Hayes et al., 2015b), hydrothermal inputs cause a preferential scavenging of Th over Pa, in contrast to opal scavenging with a fractionation factor $F \leq 1$.

A double ^{231}Pa and ^{230}Th trap

The upper meridional circulation provides a ^{231}Pa trap in the Weddell Gyre that is closely related to the nutrient trap that accumulates nutrients south of the Antarctic Polar Front and prevents their export in northward flowing mode and intermediate waters (Chase et al., 2003). Part of the diatoms with their adsorbed ^{231}Pa sink down to a lower circulation cell. The essentially complete dissolution of these sinking opal particles in the deep Weddell Sea causes a release of the ^{231}Pa (Fig 4). However, in contrast to silicate, which is exported in high concentrations in the deep AABW, ^{231}Pa is once again stripped from the water column when deep waters are flowing northward through the opal belt. Here the high dissolved ^{231}Pa activities come once again into contact with resuspended opal (see conceptual sketch in

Fig. 2). As a result, the meridional circulation in the Atlantic sector of the Southern Ocean provides a double ^{231}Pa and ^{230}Th trap, accumulating ^{231}Pa and ^{230}Th in the water column of the Weddell Gyre and in sediments of the opal belt, and yielding low ^{231}Pa and ^{230}Th concentrations in newly exported AABW.

Conclusions

Weddell Sea Bottom Water (WSBW, $\gamma_n > 28.4$ kg/m^3) is depleted in ^{230}Th and ^{231}Pa as a result of bottom water formation but, in contrast to the NADW ventilation in the North Atlantic, this water mass is too dense to leave the Weddell Sea.

In the Weddell Gyre, ^{230}Th and ^{231}Pa are removed from upwelling waters in an upper circulation cell and accumulate in WSDW ($28.4 > \gamma_n > 28.2$ kg/m^3). The release of ^{231}Pa is coupled with the near complete dissolution of opal with maximum Si and ^{231}Pa signals around 2000m.

WSDW is the Atlantic source of AABW. A mass balance shows that water leaving the Gyre exports $0.3\pm0.1 \times 10^6$ dpm s^{-1} of ^{231}Pa and $6.0\pm1.5 \times 10^6$ dpm s^{-1} of ^{230}Th, corresponding to an increase in activity of 0.04 and 0.75 dpm m^{-3}, respectively compared to inflowing waters. These enhanced activities are not found north of the ACC, and consequently they must be retained during transit of AABW through the ACC. The near-bottom depletion of ^{230}Th and ^{231}Pa observed by Deng et al. (2014) and Thomas et al. (2006) in AABW is much larger if compared with the source WSDW than if only compared with a linear extrapolation of the concentration-depth profiles.

This removal is caused and characterized by contact of outflowing deep waters with resuspended opal rich sediments in the opal belt and probably by additional scavenging by hydrothermal inputs. As a result, newly formed AABW is preconditioned by strong scavenging with very little fractionation (low F-factor). Dissolved ^{231}Pa and ^{230}Th activities are controlled by the balance between accumulation in the

Weddell Gyre and removal in the deep waters of the opal belt. If this balance would vary with the glacial-interglacial changes in productivity, opal flux and the position of the opal belt (Kumar et al., 1995) relative to the mountain ranges, it would be expected to affect the $^{231}Pa/^{230}Th$ signal recorded in deep sediments in the South Atlantic, an effect that should be considered when this signal is interpreted in terms of deep water flow.

In the meridional circulation, ^{231}Pa and ^{230}Th are removed twice in the opal belt: once in the upper circulation cell by scavenging on particles exported from surface waters and once again when outflowing deep water comes into contact with resuspended opal rich sediments.

Acknowledgments

We thank the Captain and crew of F.S. Polarstern for their help during the Zero and Drake expedition. We are grateful to the chief scientist Eberhard Fahrbach and Hein de Baar for their support and organization of the GEOTRACES program during this cruise. The manuscript was improved by thoughtful comments of four reviewers. Christoph Völker calculated the volumes of the regions distinguished in our budget calculations. We thank Mario Hoppema and Rob Middag for helpful comments on an earlier version of the manuscript. This work was funded by the DFG-Schwerpunktprogramm1158 (T11173:RU712/7-1).

References

Anderson, R.F., Bacon, M.P., Brewer, P.G., 1983. Removal of ^{230}Th and ^{231}Pa from the open ocean. Earth Planet. Sci. Lett. 62, 7-23.

Anderson, R.F., Fleisher, M.Q., Kuhn, G., Gersonde, R., Rutgers van der Loeff, M., Venchiarutti, C., submitted in parallel. An alternative view of 231Pa/230Th ratios in South Atlantic sediments.

Bacon, M.P., Anderson, R.F., 1982. Distribution of thorium isotopes between dissolved and particulate forms in the deep sea. J. Geophys. Res. 87, 2045-2056.
Biscaye, P.E., Eittreim, S.L., 1977. Suspended particulate loads and transport in the nepheloid layer of the abyssal Atlantic Ocean. Mar. Geol. 23, 155-172.
Buesseler, K.O., Ball, L., Andrews, J., Cochran, J.K., Hirschberg, D.J., Bacon, M.P., Fleer, A., Brzezinski, M., 2001. Upper ocean export of particulate organic carbon and biogenic silica in the Southern Ocean along 170°W. Deep-Sea Res. II 48, 4275-4297.
Buesseler, K.O., Barber, R.T., Dickson, M.-L., Hiscock, M.R., Moore, J.K., Sambrotto, R., 2003. The effect of marginal ice-edge dynamics on production and export in the Southern Ocean along 170°W. Deep Sea Research Part II: Topical Studies in Oceanography 50, 579.
Chase, Z., Anderson, R.F., Fleischer, M.Q., Kubik, P.W., 2002. The influence of particle composition and particle flux on scavenging of Th, Pa and Be in the ocean. Earth and Planetary Science Letters 204, 214-229.
Chase, Z., Anderson, R.F., Fleischer, M.Q., Kubik, P.W., 2003. Scavenging of ^{230}Th, ^{231}Pa and ^{10}Be in the southern ocean (SW Pacific sector): importance of particle flux, particle composition and advection. Deep-Sea Research II 50, 739-768.
DeMaster, D.J., 1981. The supply and accumulation of silica in the marine environment. Geochim. Cosmochim. Acta 45, 1715-1732.
Deng, F., Thomas, A.L., Rijkenberg, M.J.A., Henderson, G.M., 2014. Controls on seawater 231Pa, 230Th and 232Th concentrations along the flow paths of deep waters in the Southwest Atlantic. Earth and Planetary Science Letters 390, 93-102.
Fahrbach, E., Hoppema, M., Rohardt, G., Boebel, O., Klatt, O., Wisotzki, A., 2011. Warming of deep and abyssal water masses along the Greenwich meridian on decadal time scales: The Weddell gyre as a heat buffer. Deep Sea Research Part II: Topical Studies in Oceanography 58, 2509-2523.
Farley, K.A., Turekian, K.K., 1990. Lead-210 in the circumpolar South Atlantic. Deep-Sea Res. 37, 1849-1860.
Fischer, G., Fuetterer, D., Gersonde, R., Honjo, S., Osterman, D., Wefer, G., 1988. Seasonal variability of particle flux in the Weddell Sea and its relation to ice cover. Nature 335, 426-428.
Fleisher, M.Q., Anderson, R.F., 2003. Assessing the collection efficiency of Ross Sea sediment traps using ^{230}Th and ^{231}Pa. Deep Sea Research Part II: Topical Studies in Oceanography 50, 693-712.
Geibert, W., P.Assmy, Bakker, D.C.E., Hanfland, C., Hoppema, M., Pichevin, L., Schröder, M., Schwarz, J.N., Stimac, I., Usbeck, R., Webb, A., 2010. High productivity in an ice melting hotspot at the eastern boundary of the Weddell Gyre Global Biogeochem. Cycles 24, GB3007, doi:10.1029/2009GB003657, 2010.
Geibert, W., Rutgers van der Loeff, M.M., Usbeck, R., Gersonde, R., Kuhn, G., Seeberg-Elverfeldt, J., 2005. Quantifying the opal belt in the Atlantic and Southeast Pacific Sector of the Southern Ocean by means of ^{230}Th-normalization. Global Biogeochem. Cycles 19, doi:10.1029/2005GB002465.
German, C.R., Livermore, R.A., Baker, E.T., Bruguier, N.I., Connelly, D.P., Cunningham, A.P., Morris, P., Rouse, I.P., Statham, P.J., Tyler, P.A., 2000. Hydrothermal plumes above the East Scotia Ridge: an isolated high-latitude back-arc spreading centre. Earth and Planetary Science Letters 184, 241-250.
Gordon, A.L., Visbeck, M., Huber, B., 2001. Export of Weddell Sea deep and bottom water. Journal of Geophysical Research: Oceans 106, 9005-9017.
Haine, T.W.N., Watson, A.J., Liddicoat, M.I., Dickson, R.R., 1998. The flow of Antarctic bottom water to the southwest Indian Ocean estimated using CFCs. Journal of Geophysical Research: Oceans 103, 27637-27653.
Hayes, C.T., Anderson, R.F., Fleisher, M.Q., Huang, K.-F., Robinson, L.F., Lu, Y., Cheng, H., Edwards, R.L., Moran, S.B., 2015a. 230Th and 231Pa on GEOTRACES GA03, the U.S. GEOTRACES North Atlantic

transect, and implications for modern and paleoceanographic chemical fluxes. Deep Sea Research Part II: Topical Studies in Oceanography 116, 29-41.
Hayes, C.T., Anderson, R.F., Fleisher, M.Q., Vivancos, S.M., Lam, P.J., Ohnemus, D.C., Huang, K.-F., Robinson, L.F., Lu, Y., Cheng, H., Edwards, R.L., Moran, S.B., 2015b. Intensity of Th and Pa scavenging partitioned by particle chemistry in the North Atlantic Ocean. Marine Chemistry 170, 49-60.
Henderson, G.M., Heinze, C., Anderson, R.F., Winguth, A.M.E., 1999. Global distribution of the ^{230}Th flux to ocean sediments constrained by GCM modelling. Deep Sea Research Part I: Oceanographic Research Papers 46, 1861-1893.
Hoppema, M., Baar, H.J.W.d., Fahrbach, E., Bellerby, R.G.J., 2002. Renewal time and transport of unventilated Central Intermediate Water of the Weddell Sea derived from biogeochemical properties. Journal of Marine Research 60, 677-697.
Hoppema, M., Bakker, K., van Heuven, S.M.A.C., van Ooijen, J.C., de Baar, H.J.W., 2015. Distributions, trends and inter-annual variability of nutrients along a repeat section through the Weddell Sea (1996–2011). Marine Chemistry.
Hoppema, M., Dehairs, F., Navez, J., Monnin, C., Jeandel, C., Fahrbach, E., de Baar, H.J.W., 2010. Distribution of barium in the Weddell Gyre: Impact of circulation and biogeochemical processes. Marine Chemistry 122, 118-129.
Hoppema, M., Fahrbach, E., Stoll, M.H.C., de Baar, H.J.W., 1999. Annual uptake of atmospheric CO_2 by the Weddell Sea derived from a surface layer balance, including estimations of entrainment and new production. Journal of Marine Systems 19, 219-233.
Hoppema, M., Klatt, O., Roether, W., Fahrbach, E., Bulsiewicz, K., Rodehacke, C., Rohardt, G., 2001. Prominent renewal of Weddell Sea Deep Water from a remote source. Journal of Marine Research 59, 257-279.
Huhn, O., Hellmer, H.H., Rhein, M., Rodehacke, C., Roether, W., Schodlok, M.P., Schröder, M., 2008. Evidence of deep- and bottom-water formation in the western Weddell Sea. Deep Sea Research Part II: Topical Studies in Oceanography 55, 1098-1116.
Huhn, O., Rhein, M., Hoppema, M., van Heuven, S., 2013. Decline of deep and bottom water ventilation and slowing down of anthropogenic carbon storage in the Weddell Sea, 1984–2011. Deep Sea Research Part I: Oceanographic Research Papers 76, 66-84.
Jeandel, C., Rutgers van der Loeff, M., Lam, P.J., Roy-Barman, M., Sherrell, R.M., Kretschmer, S., German, C., Dehairs, F., 2015. What did we learn about ocean particle dynamics in the GEOSECS–JGOFS era? Progress in Oceanography.
Jonkers, L., Zahn, R., Thomas, A., Henderson, G., Abouchami, W., François, R., Masque, P., Hall, I.R., Bickert, T., 2015. Deep circulation changes in the central South Atlantic during the past 145 kyrs reflected in a combined 231Pa/230Th, Neodymium isotope and benthic record. Earth and Planetary Science Letters 419, 14-21.
Jullion, L., Garabato, A.C.N., Bacon, S., Meredith, M.P., Brown, P.J., Torres-Valdés, S., Speer, K.G., Holland, P.R., Dong, J., Bakker, D., Hoppema, M., Loose, B., Venables, H.J., Jenkins, W.J., Messias, M.-J., Fahrbach, E., 2014. The contribution of the Weddell Gyre to the lower limb of the Global Overturning Circulation. Journal of Geophysical Research: Oceans 119, 3357-3377.
Kretschmer, S., Geibert, W., Rutgers van der Loeff, M.M., Schnabel, C., Xu, S., Mollenhauer, G., 2011. Fractionation of 230Th, 231Pa, and 10Be induced by particle size and composition within an opal-rich sediment of the Atlantic Southern Ocean. Geochimica et Cosmochimica Acta 75, 6971-6987.
Kumar, N., Anderson, R.F., Mortlock, R.A., Froelich, P.N., Kubik, P., Dittrich-Hannen, B., Suter, M., 1995. Increased biological productivity and export production in the glacial Southern Ocean. Nature 378, 675-680.

627 Leynaert, A., Nelson, D.M., Quéguiner, B., Tréguer, P., 1993. The silica cycle in the Antarctic Ocean: is the
628 Weddell Sea atypical? Mar. Ecol. Progr. Ser. 96, 1-15.
629 Lippold, J., Gutjahr, M., Blaser, P., Christner, E., de Carvalho Ferreira, M.L., Mulitza, S., Christl, M.,
630 Wombacher, F., Böhm, E., Antz, B., Cartapanis, O., Vogel, H., Jaccard, S.L., 2016. Deep water
631 provenance and dynamics of the (de)glacial Atlantic meridional overturning circulation. Earth and
632 Planetary Science Letters 445, 68-78.
633 Lippold, J., Luo, Y., Francois, R., Allen, S.E., Gherardi, J., Pichat, S., Hickey, B., Schulz, H., 2012. Strength
634 and geometry of the glacial Atlantic Meridional Overturning Circulation. Nature Geosci 5, 813-
635 816.
636 Luo, Y., Francois, R., Allen, S.E., 2010. Sediment $^{231}Pa/^{230}Th$ as a recorder of the rate of the Atlantic
637 meridional overturning circulation: insights from a 2-D model. Ocean Sci. 6, 381-400.
638 McManus, J.F., Francois, R., Gherardi, J.-M., Keigwin, L.D., Brown-Leger, S., 2004. Collapse and rapid
639 resumption of Atlantic meridional circulation linked to deglacial climate changes. Nature 428,
640 834-837.
641 Meredith, M.P., Locarnini, R.A., Van Scoy, K.A., Watson, A.J., Heywood, K.J., King, B.A., 2000. On the
642 sources of Weddell Gyre Antarctic Bottom Water. Journal of Geophysical Research: Oceans 105,
643 1093-1104.
644 Middag, R., de Baar, H.J.W., Laan, P., Cai, P.H., van Ooijen, J.C., 2011. Dissolved manganese in the Atlantic
645 sector of the Southern Ocean. Deep Sea Research Part II: Topical Studies in Oceanography 58,
646 2661-2677.
647 Moran, S.B., Shen, C.-C., Edmonds, H.N., Weinstein, S.E., Smith, J.N., Edwards, R.L., 2002. Dissolved and
648 particulate ^{231}Pa and ^{230}Th in the Atlantic Ocean: constraints on intermediate/deep water age,
649 boundary scavenging, and $^{231}Pa/^{230}Th$ fractionation. Earth and Planetary Science Letters 203, 999-
650 1014.
651 Naveira Garabato, A.C., McDonagh, E.L., Stevens, D.P., Heywood, K.J., Sanders, R.J., 2002. On the export
652 of Antarctic Bottom Water from the Weddell Sea. Deep Sea Research Part II: Topical Studies in
653 Oceanography 49, 4715-4742.
654 Negre, C., Zahn, R., Thomas, A.L., Masqué, P., Henderson, G.M., Martínez-Méndez, G., Hall, I.R., Mas, J.L.,
655 2010. Reversed flow of Atlantic deep water during the Last Glacial Maximum. Nature 468, 84-88
656 doi:10.1038/nature09508.
657 NOAA, 1988. Data Announcement 88-MGG-02, Digital relief of the Surface of the Earth. National
658 Geophysical Data Center, Boulder, Colorado.
659 Nozaki, Y., Horibe, Y., Tsubota, H., 1981. The water column distributions of thorium isotopes in the
660 western North Pacific. Earth Planet. Sci. Lett. 54, 203-216.
661 Orsi, A.H., Johnson, G.C., Bullister, J.L., 1999. Circulation, mixing, and production of Antarctic Bottom
662 Water. Progress in Oceanography 43, 55-109.
663 Orsi, A.H., Nowlin, W.D.J., Whitworth, T.I., 1993. On the circulation an stratification of the Weddell Gyre.
664 Deep-Sea Res. 40, 169-203.
665 Orsi, A.H., Smethie, W.M., Bullister, J.L., 2002. On the total input of Antarctic waters to the deep ocean: A
666 preliminary estimate from chlorofluorocarbon measurements. Journal of Geophysical Research:
667 Oceans 107, 31-31-31-14.
668 Orsi, A.H., Whitworth, T.I., Nowlin, W.D.J., 1995. On the meridional extent and fronts of the Antarctic
669 Circumpolar Current. Deep-Sea Res.I 42, 641-673.
670 Planchon, F., Cavagna, A.-J., Cardinal, D., André, L., Dehairs, F., 2012. Late summer particulate organic
671 carbon export and twilight zone remineralisation in the Atlantic sector of the Southern Ocean.
672 Biogeosciences 9, 3423–3477.
673 Rutgers van der Loeff, M.M., Berger, G.W., 1991. Scavenging and particle flux: seasonal and regional
674 variations in the southern ocean (Atlantic sector). Mar. Chem. 35, 553-568.

675 Rutgers van der Loeff, M.M., Berger, G.W., 1993. Scavenging of ^{230}Th and ^{231}Pa near the Antarctic Polar
676 Front in the South Atlantic. Deep-Sea Res.I 40, 339-357.
677 Rutgers van der Loeff, M.M., Buesseler, K., Bathmann, U., Hense, I., Andrews, J., 2002. Comparison of
678 carbon and opal export rates between summer and spring bloom periods in the region of the
679 Antarctic Polar Front, SE Atlantic. Deep Sea Research Part II: Topical Studies in Oceanography 49,
680 3849-3869.
681 Scholten, J.C., Fietzke, J., Mangini, A., Garbe-Schönberg, C.D., Eisenhauer, A., Schneider, R., Stoffers, P.,
682 2008. Advection and scavenging: Effects on 230Th and 231Pa distribution off Southwest Africa.
683 Earth and Planetary Science Letters 271, 159-169.
684 Sloyan, B.M., Rintoul, S.R., 2001. The Southern Ocean Limb of the Global Deep Overturning Circulation*.
685 Journal of Physical Oceanography 31, 143-173.
686 Smetacek, V., De Baar, H.J.W., Bathmann, U.V., Lochte , K., Rutgers van der Loeff, M.M., 1997. Ecology
687 and biogeochemistry of the Antarctic Circumpolar Current during austral spring: a summary of
688 Southern Ocean JGOFS cruise ANT X/6 of R.V. Polarstern. Deep-Sea Res.II 44 1-21.
689 Somayajulu, B.L.K., Craig, H., 1976. Particulate and soluble 210Pb activities in the deep sea. Earth
690 Planet.Sci.Lett. 32, 268- 276.
691 Tao, C., Lin, J., Guo, S., Chen, Y.J., Wu, G., Han, X., German, C.R., Yoerger, D.R., Zhou, N., Li, H., Su, X., Zhu,
692 J., DY115-19, a.t., Parties, D.-S., 2012. First active hydrothermal vents on an ultraslow-spreading
693 center: Southwest Indian Ridge. Geology 40, 47-50.
694 Thomas, A.L., Henderson, G.M., Robinson, L.F., 2006. Interpretation of the 231Pa/230Th paleocirculation
695 proxy: New water-column measurements from the southwest Indian Ocean. Earth and Planetary
696 Science Letters 241, 493.
697 Usbeck, R., Rutgers van der Loeff, M.M., Hoppema, M., Schlitzer, R., 2002. Shallow mineralization in the
698 Weddell Gyre. Geochemistry, Geophysics, Geosystems 3, 2001GC000182.
699 Vanicek, M., Siedler, G., 2002. Zonal Fluxes in the Deep Water Layers of the Western South Atlantic
700 Ocean. Journal of Physical Oceanography 32, 2205-2235.
701 Venchiarutti, C., Rutgers van der Loeff, M., Stimac, I., 2011a. Scavenging of ^{231}Pa and thorium isotopes
702 based on dissolved and size-fractionated particulate distributions at Drake Passage (ANTXXIV-3).
703 Deep-Sea Res . II 58, 2767-2784, doi:2710.1016/j.dsr2762.2010.2710.2040.
704 Venchiarutti, C., Rutgers van der Loeff, M.M., Stimac, I., 2011b. Radionuclides measured on 21 water
705 bottle profiles during POLARSTERN cruise ANT-XXIV/3. doi:10.1594/PANGAEA.746773.
706 Walter, H.J., Rutgers van der Loeff, M.M., Höltzen, H., 1997. Enhanced scavenging of ^{231}Pa relative to
707 ^{230}Th in the South Atlantic south of the Polar Front: Implications for the use of the ^{231}Pa/^{230}Th
708 ratio as a paleoproductivity proxy. Earth Planet. Sci. Lett. 149, 85-100.
709 Walter, H.J., Rutgers van der Loeff, M.M., Höltzen, H., Bathmann, U., 2000. Reduced scavenging of ^{230}Th
710 in the Weddell Sea: Implications for paleoceanographic reconstructions in the South Atlantic.
711 Deep-Sea Res. I 47, 1369-1387.
712 Whitworth, T., Nowlin, W.D., 1987. Water masses and currents of the Southern Ocean at the Greenwich
713 meridian. J. Geophys. Res. 92, 6462-6476.
714 Yu, E.-F., Francois, R., Bacon, M.P., 1996. Similar rates of modern and last-glacial ocean thermohaline
715 circulation inferred from radiochemical data. Nature 379, 689-694.

716

717

718 Table 1. Water masses and fluxes (Sv) into and out of the indicated neutral density layers in the area

719 confined by the transects SAVE 4, Wedsea, DrakeP and AJAX (after Sloyan and Rintoul, 2001). For

720 AABW/WSDW we distinguish the deep water flowing into in the Argentine Basin (AABWA).

	Across SAVE 4		Across Wedsea		Diapycnal				Pacific/Indian	
γ^n					above		below			
$kg.m^{-3}$	in (S)	out (N)	in (N)	out (S)	in	out	in	out	in	out
<27.4		AASW 9.3±0.6						AASW 4	AASW 6.0±0.4	
27.4-28	NADW 6.7±1.4		AASW 1.0±0.2	NADW 1.0±0.2	AASW 4			NADW 1		NADW 2.2±1.1
28-28.2	LCDW 10.0±1.8			LCDW 8±2 *	NADW 1		WSDW 5			LCDW 11.9±1.9
>28.2		AABWA 6.6±1.3	WSDW 8±2 *			WSDW 5			WSDW 7.7±1.8	

721 * Jullion et al. (2014)

722 Table 2. Average activities (with ranges) of ^{230}Th and ^{231}Pa in the water masses. For AABW/WSDW we distinguish

723 between the western (WSDWW) and central/eastern (WSDWE) part of the South Atlantic and the deep water

724 flowing into in the Argentine Basin (AABWA)

	γ^n	^{230}Th	^{231}Pa	Reference
	kg.m^{-3}	dpm m^{-3}	dpm m^{-3}	
AASW-AAIW	<27.4	0.2 ± 0.09 (0.17-0.36)	0.1 ± 0.06 (0.04-0.19)	(Venchiarutti et al., 2011b, Sta 101)
NADW	27.4-28	0.4 ± 0.09 (0.31-0.67*)	0.3 ± 0.14 (0.13-0.41)	(Venchiarutti et al., 2011b, Sts 101, 104)
LCDW	28-28.2	1 ± 0.1 (0.6-1.1)	0.35 ± 0.03 (0.31-0.35)	Rutgers van der Loeff and Berger (1993)
WSDWW	28.2-28.4	1.5 ± 0.2 (1.16-1.56)	0.4 ± 0.04 (0.37-0.44)	(Venchiarutti et al., 2011a, Sta 236)
WSDWE	28.2-28.4	1.9 ± 0.2 (1.61-1.95)	0.6 ± 0.06 (0.48-0.61)	(Venchiarutti et al., 2011b, Sta 193) (WS)
AABWA	≥28.2	0.83 ± 0.2	0.28 ± 0.03	Deng et al., (2014)

725 * leaving out datapoint (1245m) with exceptionally high particulate ^{230}Th

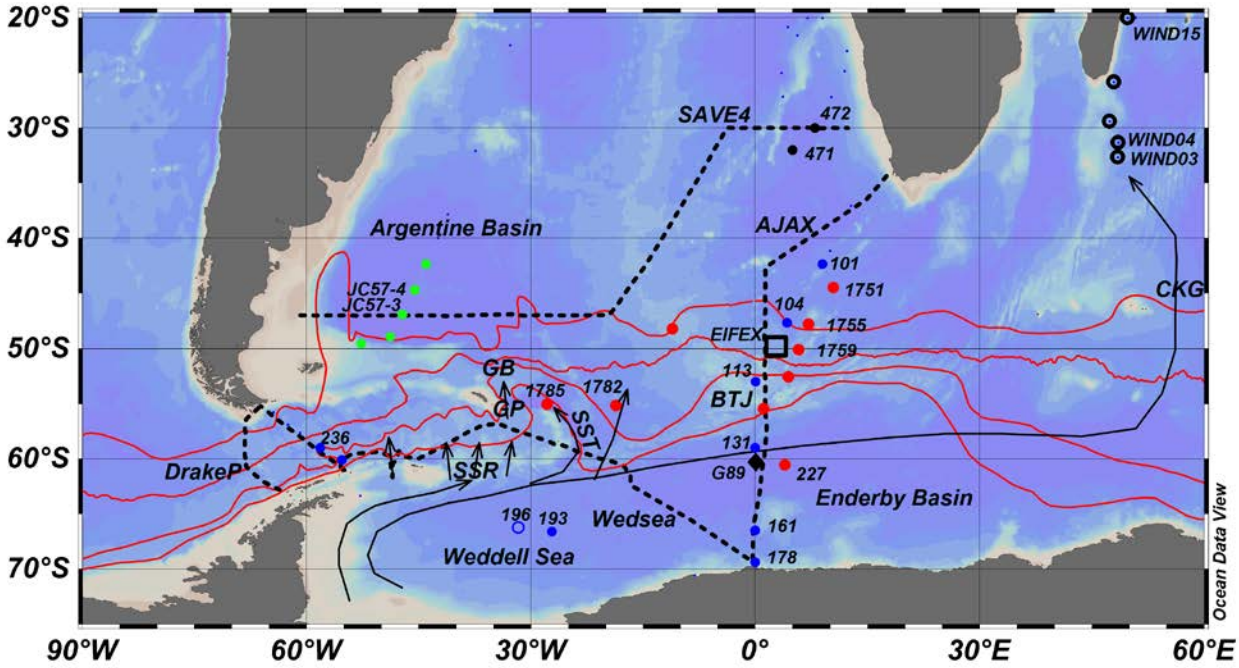

Fig. 1. Map with published hydrographic sections used to make the budget (broken lines, SAVE4, AJAX , Wedsea, DrakeP), stations of Rutgers van der Loeff and Berger (1993, red symbols), Deng et al. (2014, green symbols), Venchiarutti et al. (2011a,b, blue symbols), Huhn et al. (2013, open blue circle: station 196, data from 2008), Scholten et al. (2008, black dots), Thomas et al., (2006, black circles) and GEOSECS 89 (black diamond G89), and the location of the EIFEX study (black square) and the Bouvet Triple Junction (BTJ). Outflow pathways of AABW through four Passages in the South Scotia Ridge (SSR; from W to E: Philip, Orkney, Bruce and Discovery Passage), the Georgia Passage (GP) and Georgia Basin (GB), the South Sandwich Trench (SST) and the Crozet Kerguelen Gap (CKG) indicated by arrows. Red lines indicate average position of (from N to S) Subantarctic Front, Polar Front, Southern ACC Front and ACC Southern Boundary (Orsi et al., 1995).

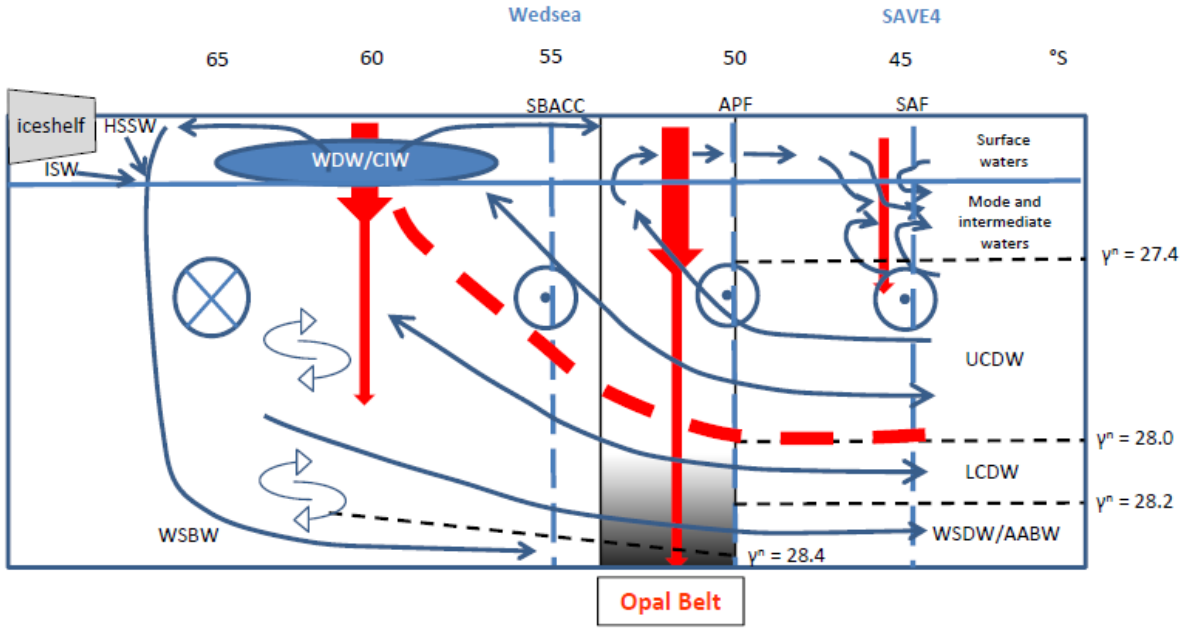

738

739 Fig. 2. Conceptual diagram of 2-D meridional circulation of the Southern Ocean after Chase et al. (2003),
740 modified to include the Weddell Gyre. The figure shows the approximate positions of the Wedsea and
741 SAVE4 sections, upper and lower circulation cells separated by the dashed red line, eastward transport
742 (circles with dots) in the ACC fronts, westward transport (circle with cross) from Indian Ocean in the
743 Antarctic Slope Front (ASF) and in-between the Central Intermediate Water (WDW/CIW, blue area).
744 Particle fluxes are indicated by red arrows, vertical mixing and isopycnal exchange by blue arrows. The
745 high opal-rich deep particle flux in the productive zone south of APF (opal belt with nepheloid layer) is
746 contrasted with the lower production zones further north and the zone with shallower mineralization in
747 the Weddell Gyre. Near the ice shelf the production of High Salinity Shelf water (HSSW) and Ice Shelf
748 Water (ISW) that mix with WDW to form WSBW is indicated.

749

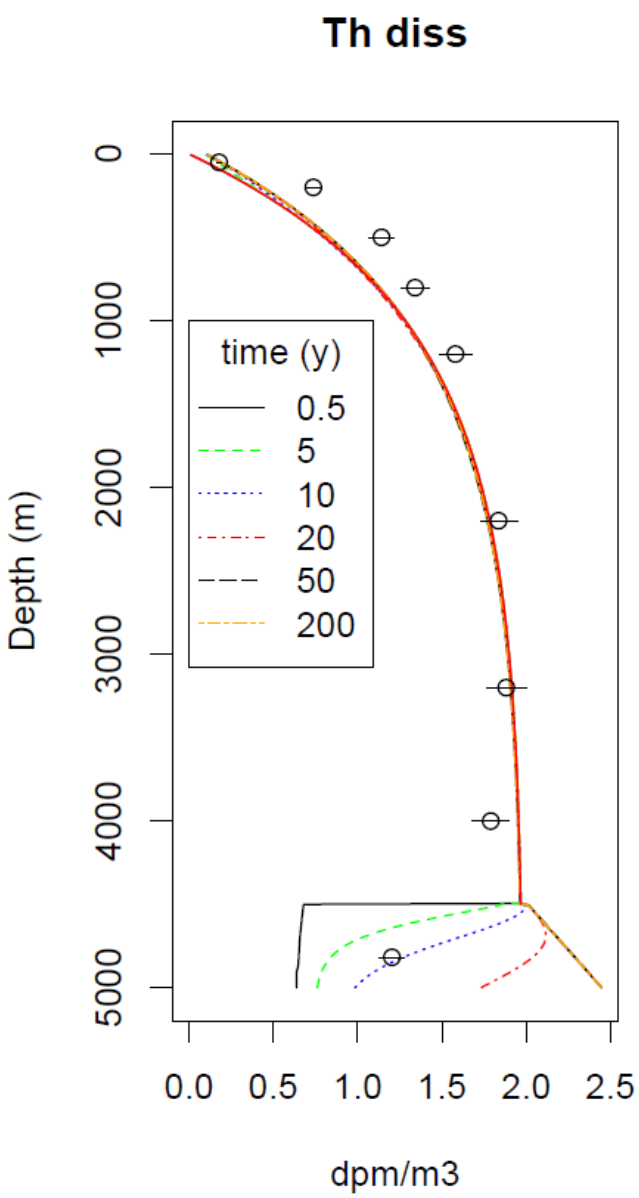

Fig. 3. Distribution of dissolved ^{230}Th (±SE) at station PS71/193 (Venchiarutti et al., 2011b) with for depth range 0-4500m the steady-state model (analytical solution in red) of Rutgers van der Loeff and Berger (1993). Below 4500m dissolved ^{230}Th follows a time-dependent model. It starts at t=0 with newly formed WSBW (see text for estimate of ^{230}Th activity) and is then allowed to develop over time by ingrowth and reversible exchange with settling particles, showing that the value measured at 4800m is reached after about 10 years. This model run does not include eddy diffusion or upwelling in the bottom layer.

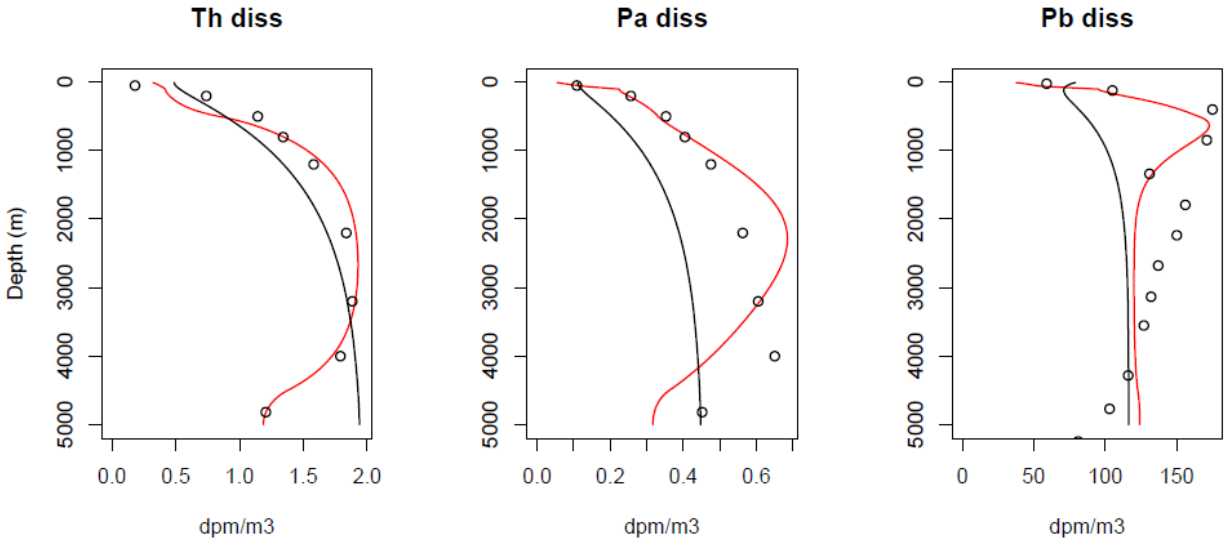

757

758 Fig.4. Distribution of dissolved ^{231}Pa, ^{230}Th (Sta 193, Venchiarutti et al., 2011b), and of ^{210}Pb (Station
759 GEOSECS 89, Somayajulu and Craig, 1976) in the Weddell Gyre (circles) compared with the model of
760 Rutgers van der Loeff and Berger (1993) including vertical mixing and, for ^{210}Pb, atmospheric input (black
761 lines). A modified model (red lines) includes ventilation of deep water by nuclide-depleted WSBW, and
762 accumulation of nuclides in an upper meridional circulation cell by rapid exchange of WDW/CIW (100-
763 500m) with UCDW/LCDW from N of Polar Front. For ^{231}Pa and ^{210}Pb, a reasonable fit with observations
764 can only be obtained by assuming an increased scavenging of Pa and Pb relative to Th in surface waters,
765 decreasing with depth with a relaxation depth of 2000m for ^{231}Pa and 250m for ^{210}Pb.

766

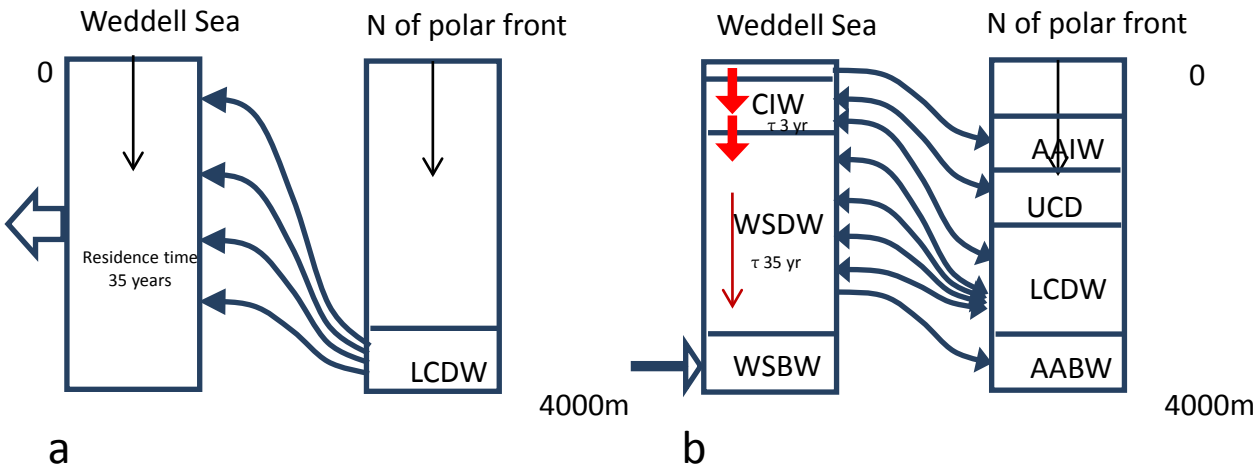

Fig. 5. Model describing upwelling and scavenging in the Southern Ocean and adjacent Weddell Gyre. (a), ^{230}Th model of Rutgers van der Loeff and Berger (1993), considering an input by upwelling of LCDW in entire water column of Weddell Gyre and a 60% reduced scavenging rate in Weddell Gyre. (b) modified model (this paper) including ventilation of Weddell Sea by WSBW, rapid exchange of WDW/CIW (100-500m) with UCDW/LCDW from N of Polar Front (Hoppema et al., 2002), and a scavenging term in the Weddell Gyre that is constant for Th but depth-dependent for Pa and Pb.

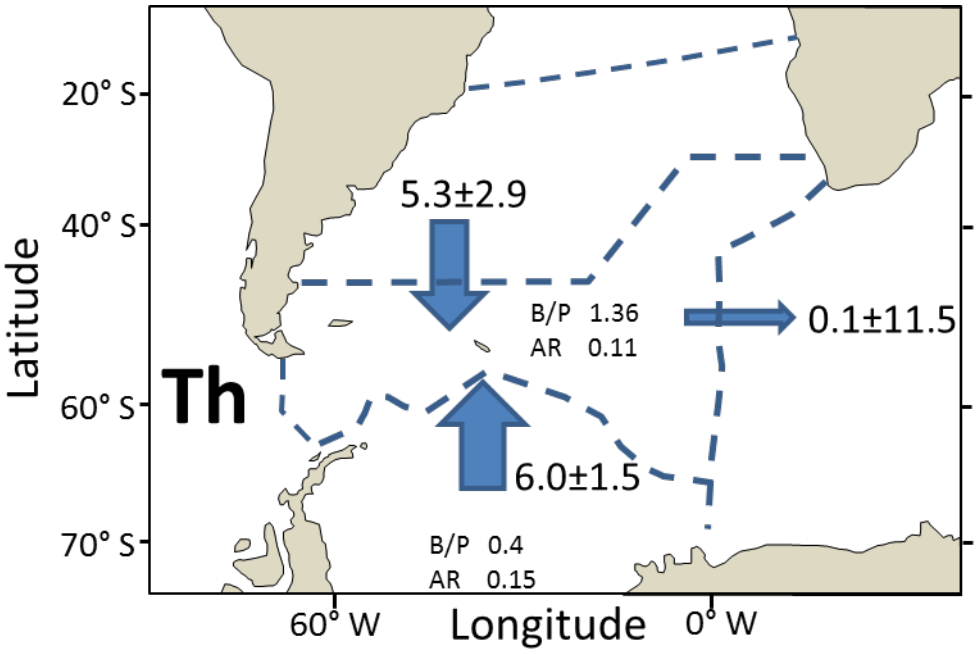

776

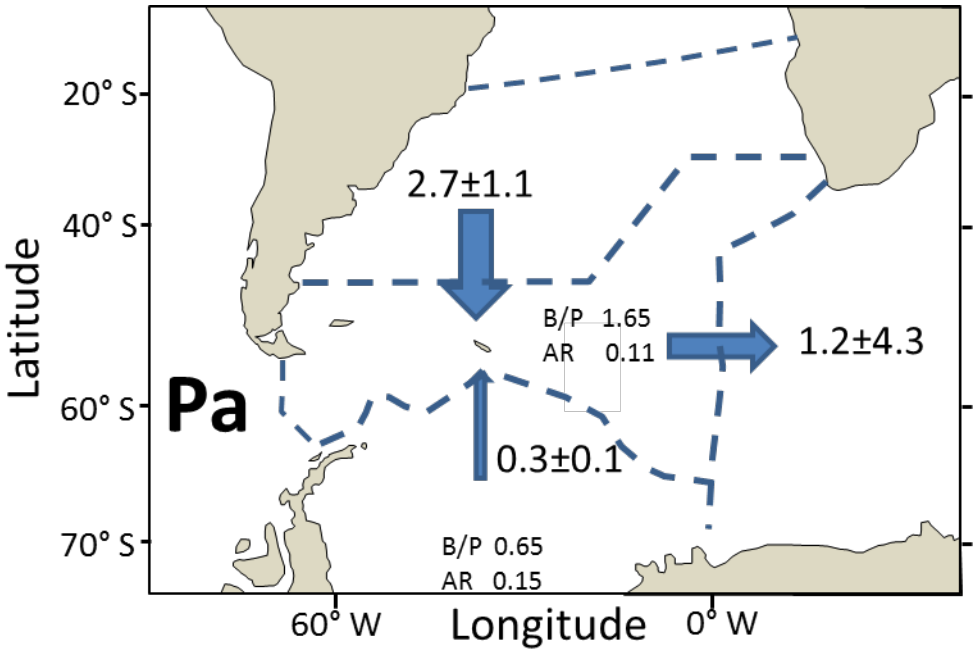

777

778 Fig.6. Balance of ^{230}Th (a) and ^{231}Pa (b) activities based on circulation model of Sloyan and Rintoul (2001)

779 (Table 1) and radionuclide activities from Table 2. Fluxes from Weddell Sea based on production and

780 sedimentation constraints in Weddell Gyre. Arrows: Net fluxes with SE (10^6 dpm s^{-1}). B/P:

burial/production ratio. AR: Pa/Th burial activity ratio. Flux to Indian Ocean represents excess over input from Pacific Ocean.

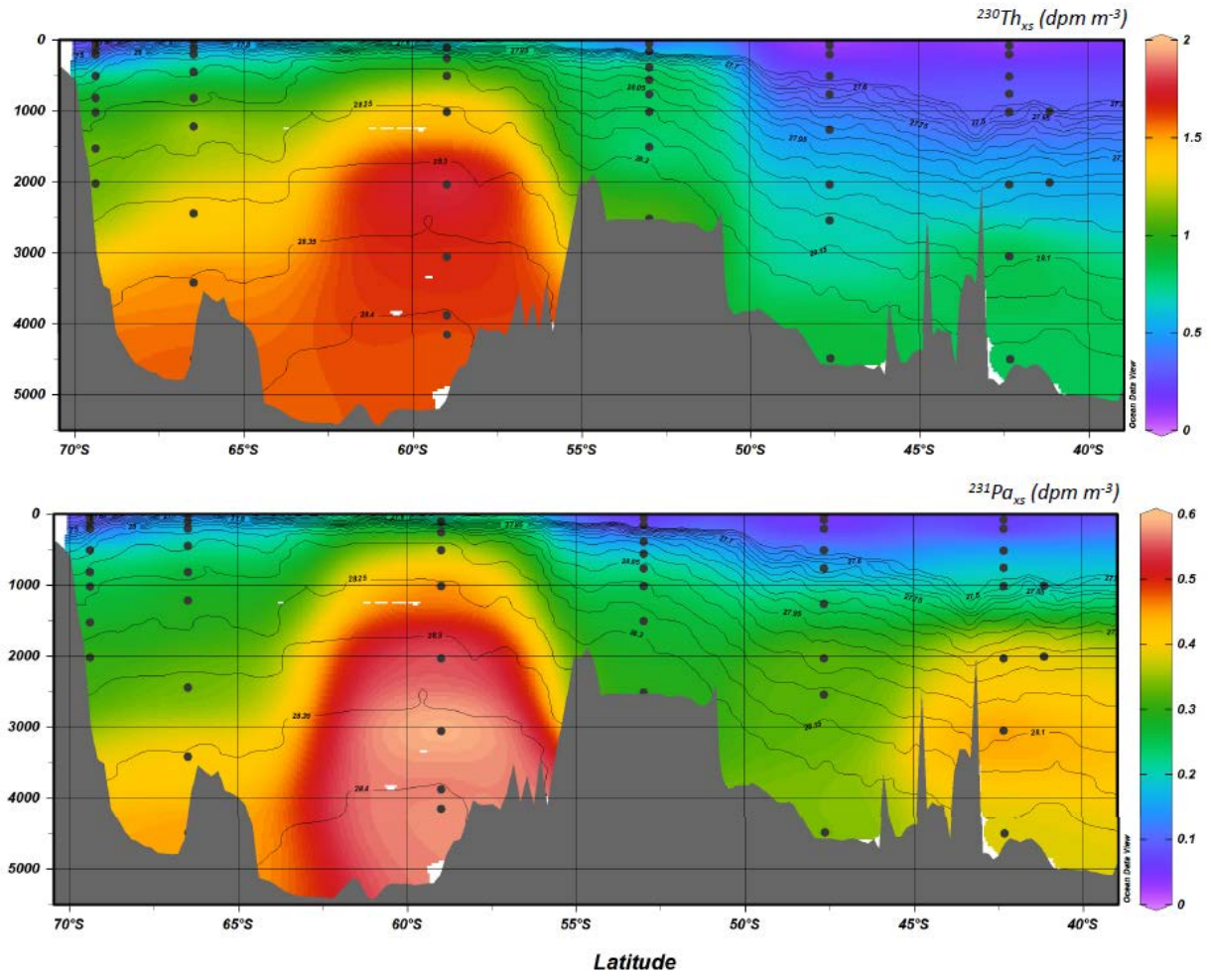

Fig.7 Vertical section along the Zero Meridian of excess dissolved ^{230}Th and ^{231}Pa (dpm/m3, from Venchiarutti et al., 2011b) with contours of neutral density anomaly (kg m^{-3}) showing accumulation of ^{230}Th and ^{231}Pa in the Weddell Gyre.

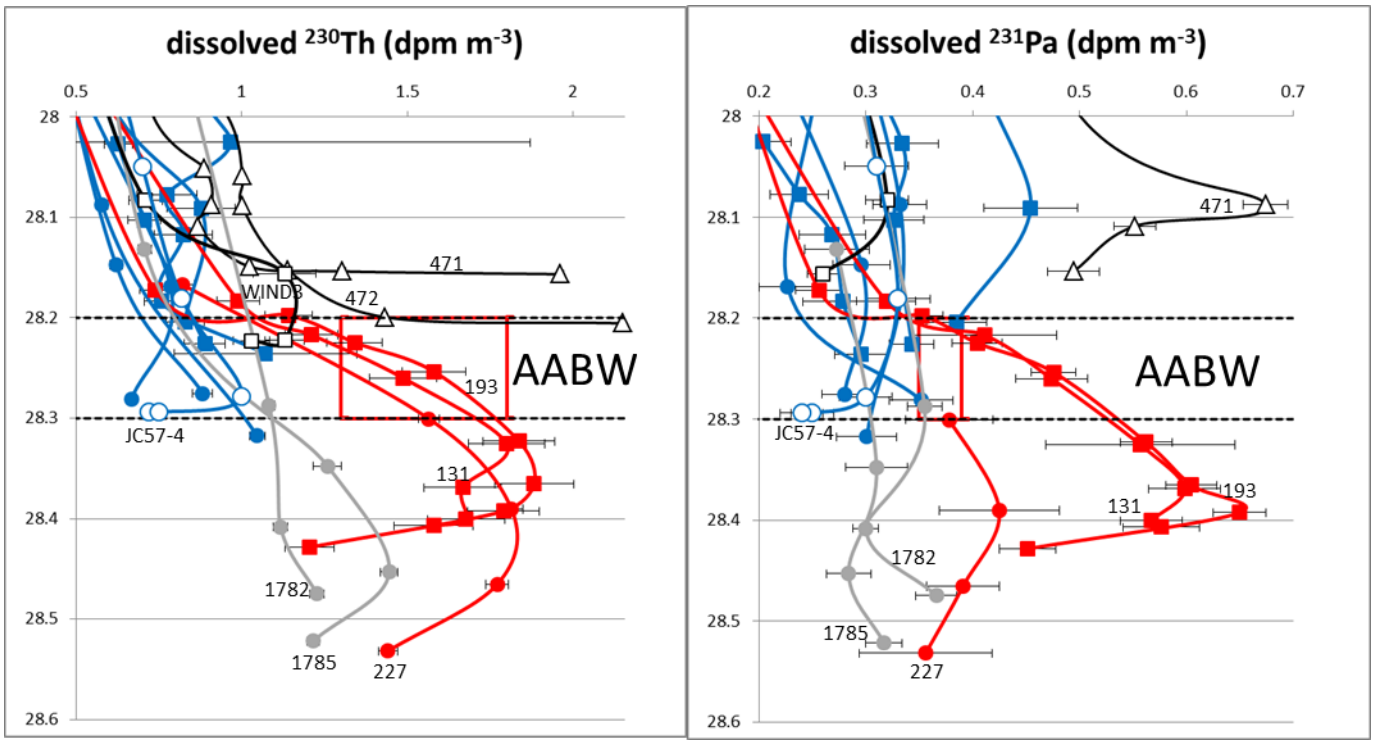

788

789 Fig 8. Dissolved ^{230}Th and ^{231}Pa activities in the neutral density range (kg m^{-3}) of the AABW outflow.
790 Observed activities (Deng et al., 2014, open circles; Rutgers van der Loeff and Berger, 1993, filled circles;
791 Venchiarutti et al., 2011b, filled squares) north of the APF (blue) are much lower than activities observed in
792 the Weddell Gyre (red) and those expected for outflowing AABW based on the mass balance of the Weddell
793 Gyre (boxes as described in text). Black symbols and lines represent observations in the Cape Basin
794 (Scholten et al., 2008, open triangles; sta 472 refers to total concentrations) and the SW Indian Ocean
795 (Thomas et al., 2006, open squares). Grey symbols are profiles observed close to the APF at stations 1782
796 and 1785 (Fig. 1, Rutgers van der Loeff and Berger, 1993).

797